FREQUENCY DISTRIBUTIONS AND CORRELATIONS OF SOLAR X-RAY FLARE PARAMETERS

NORMA B. CROSBY[1,2], MARKUS J. ASCHWANDEN[1,3], and BRIAN R. DENNIS[1]

(Received 15 April, 1992; in revised form 21 August, 1992)

Abstract. We have determined frequency distributions of flare parameters from over 12000 solar flares recorded with the Hard X-Ray Burst Spectrometer (HXRBS) on the Solar Maximum Mission (SMM) satellite. These parameters include the flare duration, the peak counting rate, the peak hard X-ray flux, the total energy in electrons, and the peak energy flux in electrons (the latter two computed assuming a thick-target flare model). The energies were computed above a threshold energy between 25 and 50 keV. All of the distributions can be represented by power laws above the HXRBS sensitivity threshold. Correlations among these parameters are determined from linear regression fits as well as from the slopes of the frequency distributions. Variations of the frequency distributions were investigated with respect to the solar activity cycle.

Theoretical models for the frequency distribution of flare parameters depend on the probability of flaring and the temporal evolution of the flare energy build-up. Our results are consistent with stochastic flaring and exponential energy build-up, with an average build-up time constant that is 0.5 times the mean time between flares. The measured distributions of flares are also consistent with predicted distributions of flares from computer simulations of avalanche models that are governed by the principle of self-organized criticality.

1. Introduction

Frequency distributions have been extensively reported for various solar flare phenomena. Studies have been done on radio bursts (Akabane, 1956), soft X-rays (Hudson, Peterson, and Schwartz, 1969; Drake, 1971), hard X-rays (Datlowe, Elcan, and Hudson, 1974; Lin *et al.*, 1984; Dennis, 1985; Aschwanden and Dennis, 1992), interplanetary type III bursts (Fitzenreiter, Fainberg, and Bundy, 1976), and interplanetary particle events (Van Hollebeke, Sung, and McDonald, 1975; Cliver *et al.*, 1991). All these distributions can be represented above the sensitivity threshold by power laws of the form

$$dN = Ax^{-\alpha}\,dx\,, \tag{1}$$

where dN is the number of events recorded with the parameter x of interest between x and $x + dx$, and A and α are constants determined from a least-squares fit to the data.

[1] Laboratory for Astronomy and Solar Physics, NASA/Goddard Space Flight Center, Greenbelt, MD 20771, U.S.A.
[2] The Catholic University of America, Washington, DC 20064, U.S.A.
[3] The University of Maryland, Astronomy Department College Park, MD 20742, U.S.A.

Solar Physics **143:** 275–299, 1993.
© 1993 *Kluwer Academic Publishers. Printed in Belgium.*

Integral frequency distributions of the form

$$N(>x) = \int_x^\infty dN = \int_x^\infty Ax^{-\alpha}\,dx = \frac{A}{\alpha - 1}\,x^{-\alpha+1} \quad \text{for } \alpha > 1 \tag{2}$$

are best for studies with poor statistics. The differential distributions are preferable as all bins of the histograms are independent of each other, thus allowing the power-law fit and the uncertainties to be calculated using standard least-squares procedures.

A summary of the results of previous work on the frequency distributions of different measures of flare sizes in different wavelength ranges and particle energies is given in Table I.

While previous studies generally present only the frequency distribution of the peak count rate or peak flux of flare-related emission at a specific wavelength, we examine here a more comprehensive set of flare parameters for the hard X-ray (HXR) energy range above 25 keV. We present the frequency distributions of directly measured parameters, such as the HXR peak count rate and total flare duration, but also the distributions of derived energy-integrated parameters, such as the peak HXR photon flux and the peak HXR electron flux, and the time-integrated total flare energy, in terms of the thick-target model. Most of the parameters show an approximate power-law distribution over several orders of magnitude. We investigate also correlations among the flare parameters by means of scatter plots and functional dependences derived from the frequency distributions. In particular, we find a strong correlation between the total thick-target energy W of a flare and the product of the peak energy flux F times the flare duration D, i.e., $F \times D \sim W^{1.18}$. This relation provides useful estimates of the total flare energy based merely on measurements of F and D, without requiring the tedious spectral-dependent time integration.

Several theoretical approaches have been developed to explain the frequency distributions of flare-related parameters. Rosner and Vaiana (1978) proposed a model based on the stochastic probability of flaring and the assumption of exponential energy build-up. This model predicts a power-law distribution for flare energies sufficiently high above the quiescent energy level. Lu and Hamilton (1991) used 'avalanche theory' to relate the power-law distributions of flaring parameter to the scale-invariant properties of self-organizing systems in a critical state. Applying Parker's (1988) model of magnetic reconnection for flux tubes twisted above some critical shear angle, Lu and Hamilton obtained power-law frequency distributions in the total released energy, peak energy release rate, and time duration for such relaxation processes. The values obtained from their numerical simulations match closely our observed values but they are somewhat model-dependent, i.e., the slope of the resulting distributions depends on the assumed critical threshold for energy release. Aschwanden and Klimchuk (1992) discuss the relation of the power-law slope of the frequency distribution to flare energy storage. Based on theoretical simulations of the energy build-up phase in three-dimensional magnetic loops, they calculated theoretical distributions of the dissipated magnetic energy in flares. The evolution of the flare energy release process itself can be modeled

TABLE I

Summary of frequency distributions of different flare parameters

Reference	Parameter and units	Energy or frequency	Observatory	Power-law slope ($-\alpha$)
Hard X-rays:				
Datlowe, Elcan, and Hudson (1974)	peak flux ph $cm^{-2} s^{-1} keV^{-1}$	10–300 keV	OSO-7	– 1.8*
Lin *et al.* (1984)	peak flux ph $cm^{-2} s^{-1} keV^{-1}$	13–600 keV	balloon flight	– 2.0*
Dennis (1985)	peak rate counts s^{-1}	25–500 keV	HXRBS/SMM	– 1.8
Aschwanden and Dennis (1992)	peak rate counts s^{-1}	26–500 keV	HXRBS/SMM flare substructures	– 1.54
Soft X-rays:				
Hudson, Peterson, and Schwartz (1969)	peak flux counts $cm^{-2} s^{-1}$	7.7–12.5 keV	OSO-III	– 1.84*
Drake (1971)	peak flux ergs $cm^{-2} s^{-1}$	1–6 keV	EXPLORER 33 and 35	– 1.75
	fluence ergs cm^{-2}			– 1.44
Radio:				
Akabane (1956)	radio bursts W $cm^{-2} s^{-1} Hz^{-1}$	3 GHz	Ottawa Toyokawa Tokyo	– 1.8
Fitzenreitner, Fainberg, and Bundy (1976)	type III bursts W $m^{-2} Hz^{-1}$	815 kHz	IMP-VI	– 1.5
Interplanetary particle events:				
Van Hollebeke, Sung, and McDonald (1975)	protons $cm^{-2} s^{-1} sr^{-1} MeV^{-1}$	4–20 MeV	IMP-IV and V	– 1.15
Cliver *et al.* (1991)	protons $cm^{-2} s^{-1} sr^{-1} MeV^{-1}$	24–34 MeV	IMP-VIII	– 1.13
	electrons $cm^{-2} s^{-1} sr^{-1} MeV^{-1}$	3.6–18.5 MeV		– 1.30
Avalanche model:				
Lu and Hamilton (1991)	dissipated energy			– 1.4
	peak dissipation rate			– 1.8

* Calculated from the integral frequency distribution (Equation (2)).

as a magnetic relaxation process characterized by the logistic equation (Aschwanden, 1992). This model predicts the relation $W \sim F \times T$ (T being the duration of significant energy dissipation), similar to the relation $W^{1.18} \sim F \times D$ (D being the duration of the entire flare) empirically found in the present analysis.

The plan of our paper is the following: observations are described in Section 2, the frequency distributions and correlations are presented in Section 3, a comparison with

previous results and discussion in terms of theoretical flare models is given in Section 4, and an observational summary and conclusions follow in Section 5.

2. Observations

2.1. Hard X-ray observations

Solar flare events were recorded with the Hard X-Ray Burst Spectrometer (HXRBS) on the Solar Maximum Mission (SMM) satellite from February 19, 1980 through November 21, 1989. This instrument consists of a CsI(Na) scintillation spectrometer with a large anticoincidence shield (Orwig, Frost, and Dennis, 1980). The number of counts measured in each of 15 pulse-height channels was recorded with a time resolution of 128 ms. As a result of operational and instrumental changes in gain, the energy range covered by these channels varied from 25 to 438 keV after launch to 52 to 861 keV near the end of the mission (Dennis *et al.*, 1991). Thus, flares with energies below ~ 50 keV were detected with lower efficiency in the later years. The gain change occurred primarily in two discrete steps (in September 1985 and November 1988), probably because of loss of optical contact between the photomultiplier tubes (PMTs) and the CsI(Na) scintillator. The HXRBS FWHM energy resolution was $\sim 70\%$ at 60 keV early in the mission and was assumed to vary as $E^{0.75}$. Towards the end of the mission in 1989 after the gain changes, it is believed that the resolution had degraded to $\sim 110\%$ at 60 keV.

During the search through the original HXRBS data, the selection of solar flares was based on visual inspection, using the criterion of a significant (25%) increase in the Channel 2 counting rate lasting for ~ 10 s above the average background level (for details see Dennis *et al.*, 1991). Any increase was examined with finer time resolution and recorded as an event unless it lasted for only one 128-ms interval, in which case it was considered to be a noise pulse. The sensitivity of this search procedure was such that all flares with peak rates of > 100 counts s^{-1} were recorded with a probability close to 100%, but that weaker flares were recorded with decreasing probability. This lower probability is manifested as the roll-over for smaller events in the frequency distributions shown in Figures 2 to 7.

2.2. Selection of data

As the main database for our analysis, we used the complete HXRBS catalog from 1980 to 1989, containing a total of 12776 HXRBS events (Dennis *et al.*, 1991). Additional information from other instruments on SMM and on GOES has been compiled for 1980 by Speich *et al.* (1991). We made use of the entire dataset for the frequency distributions of the peak rate (Figure 2) and total flare duration (Figure 7), while a smaller subset was used for the frequency distributions of spectral-dependent HXR parameters.

Figure 1 shows the number of solar flare events per day that were identified for each half year of observation. The flare rate per day in Figure 1 and in the following plots has been corrected for the instrument duty cycle. This was determined from the following criteria: (i) the spacecraft had to be in the day-time part of the orbit, (ii) the

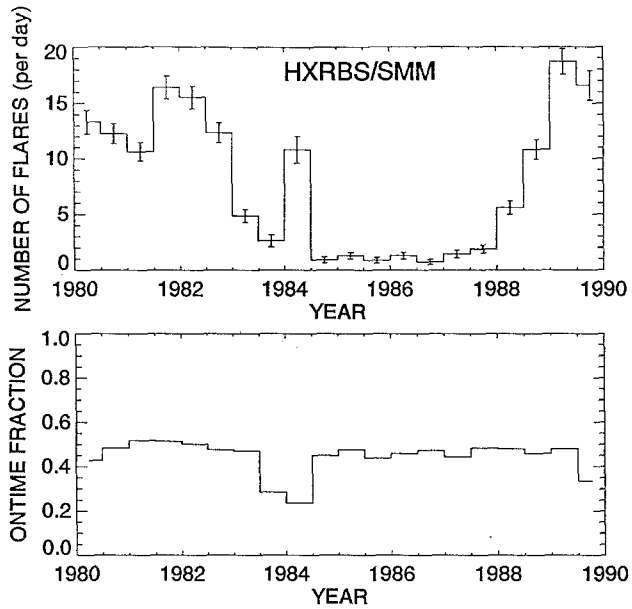

Fig. 1. True rate of flares recorded with HXRBS as a function of time from instrument turn-on on February 19, 1980, to the end of the mission on November 22, 1989. The plotted flare rate was calculated by dividing the total number of flares recorded in each half-year interval by the total time during each interval that HXRBS was actually sensitive to solar X-rays (referred to as the 'on-time'). The on-time fraction is plotted in the lower half of the figure. The ~ 9.5 years of operation was divided into the following four intervals for the subsequent analysis: 1980–1982,1983–1984, 1985–1987, and 1988–1989.

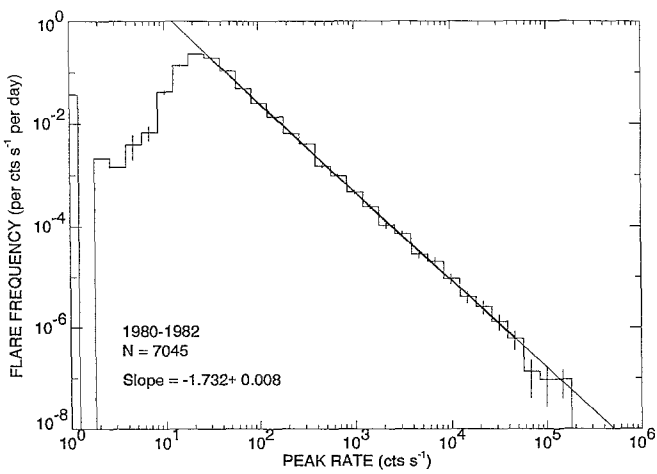

Fig. 2. The frequency distribution of the peak rate corrected for on-time is shown for all 7045 HXRBS flares recorded in 1980–1982. The error bars represent $\pm 1\sigma$ uncertainties based on Poisson statistics on the number of flares in each bin. The straight line through the points above 30 counts s^{-1} represents the least-squares fitted power-law function with a slope of -1.732 ± 0.008. The turnover below 30 counts s^{-1} corresponds to the HXRBS sensitivity limit. An average background of 40 counts s^{-1} was subtracted from the peak rate (including background) listed in the HXRBS catalog (Dennis *et al.*, 1991).

high voltage was turned on (it was turned off while passing through the SAA), (iii) the Sun had to be in the field-of-view, and (iv) the data had to be transmitted and recorded on the HXRBS computer or by the Information Processing Division (IPD) at Goddard. In 1983 and early 1984 the on-board tape recorder was being preserved for the SMM repair mission and data was only retrieved during real time contact with a ground station.

For the frequency distributions of spectral-dependent parameters, we used 8194 events (64% of the entire data set) for which power-law spectral fits were available from an automatic procedure that had been used for all events. The relevant spectral parameters were stored in 'summary files'. Spectral fits and summary files were generally produced when the peak count rate was greater than 100 counts per second or when the total duration of the event was longer than 200 seconds (see exceptions in Dennis *et al.*, 1991; p. 13). Noisy data and non-solar events were systematically excluded, reducing the dataset with good spectral parameters to 6243 events (49% of the entire data set). Most of the events where a spectral fit was not obtained were weak events with peak rates ≤ 100 counts s^{-1}. Of the bigger events, 88% of those with a peak rate ≥ 100 counts s^{-1} and 92% with ≥ 1000 counts s^{-1} have spectral fits. We tested the representativeness of our data selection by comparing the frequency distribution of the peak rate of the selected events with that for all events and do not find a systematic bias above a threshold of 100 counts s^{-1} (see Section 3.2).

In order to study the changes in the frequency distributions with time during the solar cycle and with the changes in the instrumental gain, we subdivided the data set into four groups covering the following years: 1980–1982, 1983–1984, 1985–1987, and 1988–1989. The first subset from 1980–1982 contains the largest homogeneous subset (2878 events) and is least affected by instrumental changes. Figures 3 and 5 through 11 refer to this subset.

2.3. Spectral fit procedure

The spectral fits were made using an automatic analysis procedure (DCPFIT) that involved the following steps:

(1) A file was first created containing the raw HXRBS data from the flare itself and also from before and after the flare for background estimation. The number of counts in each of the 15 pulse-height channels were included in this file together with the live time every 128 ms and all the housekeeping data.

(2) Time intervals during the flare were marked for detailed spectral analysis. They were selected such that each interval had at least 400 counts, or the count rate differed from that in the immediately preceding or following interval by more than 2.6σ calculated assuming Poisson statistics.

(3) For each interval during a flare, a count rate spectrum was accumulated and the background spectrum subtracted. A background spectrum was computed for each interval by interpolation from the pre- and post-flare intervals selected for this purpose.

(4) This count rate was deconvolved to approximate the incident photon flux, using deconvolution tables (conversion factors) previously generated by detector response

modeling software assuming a given power-law slope for the incident photon spectrum. For a more detailed description, see Batchelor (1984) and Schwartz *et al.* (1991).

(5) A least-squares fit of a function was performed, and the fit parameters and the spectrum were recorded in the summary file for that specific flare. The single power-law fit is defined as

$$I(E) = \frac{\mathrm{d}\Phi(E)}{\mathrm{d}E} = A\left(\frac{E}{E_m}\right)^{-\gamma} \text{ photons cm}^{-2}\,\text{s}^{-1}\,\text{keV}^{-1}, \tag{3}$$

where $I(E)$ is the photon flux at an energy E in keV, $\mathrm{d}\Phi(E)$ is the photon intensity between energies of E and $E + \mathrm{d}E$, E_m the mean photon energy (here 50 keV), and A and γ are free parameters.

(6) Steps 4 and 5 for each flare interval were repeated using the new power-law slope γ in the deconvolution process until the derived value for each parameter differed by less than 10% from its value on the previous iteration (approximately the uncertainty in each parameter). Best-fit results from one cycle were used as input to the next cycle.

3. Data Reduction and Results

We analyzed three groups of HXR parameters: (i) directly observed parameters such as the peak count rate (Section 3.1) and the total flare duration (Section 3.5), (ii) spectral-dependent parameters which could only be determined for those events for which a spectral fit was obtained, e.g., the peak HXR photon flux (Section 3.2), and (iii) model-dependent HXR parameters, e.g., the peak energy flux (Section 3.3) and the total flare energy (Section 3.4). In order to estimate the amount of energy deposited by HXR-emitting electrons in a flare, we used the thick-target model and the spectral parameters from the power-law fits. Frequency distributions and correlations are described in the Sections 3.1–3.6. Solar cycle and instrumental effects are discussed in Section 3.7.

3.1. Peak rate (P)

Frequency distributions of the peak rate can be well represented by a power-law over more than 3 orders of magnitude. The distribution shown in Figure 2 is for the subset of all flares recorded in 1980–1982. This is the most homogeneous subset of the data and gives a slope of -1.73 ± 0.01. The turn-over in the peak-rate frequency distribution (Figure 2) for small flares results from the reduced efficiency of finding events below a background-subtracted peak count rate of ~ 30 counts s^{-1}.

We have verified that the selection of only those events for which spectral fits could be obtained does not introduce a change in the slope of the frequency distribution by noting that the frequency distribution of the peak rate of all flares between 1980 and 1989 shows a power-law above 100 counts s^{-1} with a slope of -1.710 ± 0.012, while the corresponding distribution of events with spectral fits (49% of all events) shows a slope of 1.706 ± 0.014. Thus, we can consider events with spectral fits as representative of all events above a threshold of ~ 100 counts s^{-1}.

The slope varies between -1.67 and -1.73 for various subsets of different years (see Table II). The best value of -1.73 is slightly below the slope of -1.8 given in Dennis

TABLE II

Slope of power-law fits to the frequency distributions of HXR flare parameters

Parameter (units)	Range of fit	1980–1982	1983–1984	1985–1987	1988–1989
No. of events		7045	1008	545	3874
P – peak rate (counts s^{-1})	$60–5 \times 10^4$	-1.73 ± 0.01	-1.71 ± 0.04	-1.68 ± 0.07	-1.67 ± 0.03
	$2000–5 \times 10^4$	-1.66 ± 0.03			
D – duration (s)	200–3000	-2.17 ± 0.05	-1.95 ± 0.09	-2.22 ± 0.13	-1.99 ± 0.06
	500–3000	-2.54 ± 0.05			
No. of events with spectral fits		2878	399	331	2635
I (25 keV) peak HXR differential flux (ph $cm^{-2} s^{-1} keV^{-1}$)	0.3–50	-1.62 ± 0.02	-1.65 ± 0.06	-1.58 ± 0.03	-1.56 ± 0.03
	5–50	-1.62 ± 0.06			
Φ (>25 keV) peak HXR integral flux (ph $cm^{-2} s^{-1}$)	1.5–1000	-1.59 ± 0.01	-1.56 ± 0.05	-1.53 ± 0.03	-1.52 ± 0.03
	50–1000	-1.71 ± 0.05			
F (>25 keV) peak electron energy flux (ergs s^{-1})	$10^{27}–10^{29}$	-1.67 ± 0.04	-1.73 ± 0.07	-1.60 ± 0.05	-1.52 ± 0.03
	$10^{28}–10^{29}$	-1.68 ± 0.09			
W (>25 keV) total energy in electrons (ergs)	$3 \times 10^{28}–10^{31}$	-1.53 ± 0.02	-1.51 ± 0.04	-1.48 ± 0.02	-1.53 ± 0.02
	$5 \times 10^{29}–10^{31}$	-1.53 ± 0.03			

(1985), which can be explained by the selection criterion of Dennis (1985), where only complete events (with a duration of less than the 60-min daytime part of the SMM orbit) were included.

3.2. Peak hard X-ray flux (Φ)

By deconvolving the instrumental response of the HXRBS detector and the assumption of a power-law spectrum, we obtained the peak HXR photon flux $I = d\Phi/dE$ at a given photon energy (Equation (3)), e.g., at 25 keV, using the automatic spectral fit procedure described in Section 2.3. The hard X-ray photon flux in time interval i integrated above a cut-off energy of E_0, $\Phi_i(>E_0)$, is of the form

$$\Phi_i(>E_0) = \frac{A_i E_m}{(\gamma_i - 1)} \left(\frac{E_0}{E_m}\right)^{-\gamma_i + 1} \text{ photons cm}^{-2}\,\text{s}^{-1}\,. \tag{4}$$

The peak hard X-ray flux refers to the time interval during the flare when the total count rate was highest.

The frequency distribution of the peak HXR photon flux I at 25 keV has a slope of -1.62 ± 0.02, while the peak integrated HXR photon flux Φ (>25 keV), shown in Figure 3, has a slope of 1.59 ± 0.01. Both frequency distributions show a power law

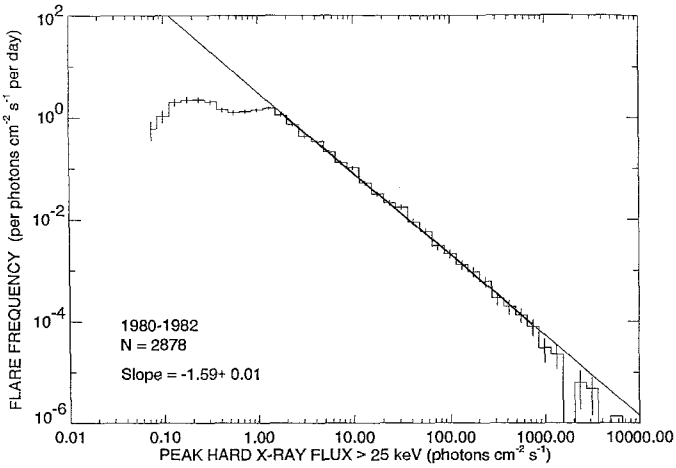

Fig. 3. The frequency distribution of the peak hard X-ray flux above 25 keV, calculated for those 2878 flares in 1980–1982 with sufficient count rate to enable a power-law spectral fit to be made on the data. The number of events is corrected for on-time. The slope of the weighted power-law fit is -1.59 ± 0.01.

over three decades in flux. The similarity of these slopes with that of the frequency distribution for the peak count rate indicates that there is nearly a one-to-one conversion between these parameters, although there is a slight spectral dependence on the peak count rate (the spectral slope tends to be flatter for events with higher count rate; Dennis, 1985). The functional dependence among these parameters is discussed below in Section 3.6 and tabulated in Table III.

The slope of the frequency distribution of the peak HXR photon flux varies between -1.52 and -1.73 during the years from 1980 to 1989 (see Table II), reaching the flattest slope in 1989 at the end of the SMM mission. In Section 3.7, we discuss possible effects of instrumental changes that may have caused or contributed to these changes in slope.

In Figure 4 we compare the integral rate of occurrence of events vs peak hard X-ray flux at 20 keV (photon cm^{-2} s^{-1} keV^{-1}) to that reported by Lin *et al.* (1984, 1991) and by Datlowe *et al.* (1974). The hard X-ray flux at 20 keV was obtained from the HXRBS data by extrapolating the single power-law fit downward in energy from the range above 25–30 keV covered by that instrument. The flare frequency drops about a factor of 10 during the solar cycle minimum. The turnover at $\Phi_{20} < 0.5$ photons cm^{-2} s^{-1} is caused by the reduced probability for flare detection with count rates <100 counts s^{-1}.

As shown in Figure 4, Lin's data from both balloon flights are fully consistent with the extrapolated flare frequency distributions measured with HXRBS at the corresponding phases of the solar cycle. The distribution obtained from the 25 microflares

TABLE III

Power-law exponents of correlated HXR flare parameters

Correlation function		All flares*			Strong flares*		
		CC	Exponent – a		CC	Exponent – a	
			Linear regression method	Frequency distribution method		Linear regression method	Frequency distribution method
D	$\sim P^a$	0.32	0.45 ± 0.03	0.59 ± 0.05	0.28	0.43 ± 0.04	0.41 ± 0.04
I (25 keV)	$\sim P^a$	0.93	1.01 ± 0.01	1.10 ± 0.04	0.93	0.95 ± 0.01	1.06 ± 0.10
Φ (> 25 keV)	$\sim P^a$	0.95	1.07 ± 0.01	1.13 ± 0.04	0.95	1.02 ± 0.01	0.93 ± 0.08
F (> 25 keV)	$\sim P^a$	0.84	0.94 ± 0.02	1.00 ± 0.05	0.82	0.89 ± 0.02	0.97 ± 0.14
W (> 25 keV)	$\sim P^a$	0.79	1.25 ± 0.02	1.31 ± 0.03	0.75	1.21 ± 0.03	1.25 ± 0.09
$F \times D$ (> 25 keV)	$\sim P^a$	0.77	1.48 ± 0.03	1.59 ± 0.10	0.80	1.30 ± 0.04	1.38 ± 0.17
$F \times D$ (> 25 keV)	$\sim W^a$	0.92	1.18 ± 0.01	1.21 ± 0.08	0.80	1.03 ± 0.05	1.11 ± 0.14

CC – correlation coefficient of linear regression (in log-log space).

* The power-law exponent (a) of the correlated parameters was determined by the orthogonal linear regression method, excluding data points below a separatrix intersecting the regression line at 100 counts s^{-1} (for 'all flares') and 200 counts s^{-1} (for 'strong flares'). The slope of the frequency distribution for each parameter was determined by fitting a power-law function over the wide parameter range given in Table II in the case of 'all flares', and over the upper range (defined in Table II) for the case of 'strong flares'.

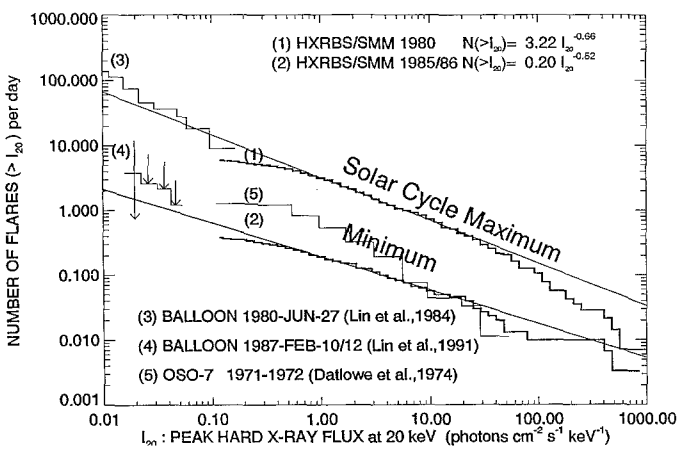

Fig. 4. The integral rate of occurrence of events vs peak X-ray flux at 20 keV for the following four data sets: from OSO-7 (Datlowe *et al.*, 1974), from the balloon-borne 300 cm^2 NaI/CsI phoswich scintillator (Lin *et al.*, 1974; Lin *et al.*, 1991), and from HXRBS/SMM (this work). The HXRBS data set is broken down into 2 subsets, for a period near the solar cycle maxima (1980 and 1989), and for a period near the solar cycle minimum (1985–1986). The data points of Lin *et al.* (1991) represents 2σ upper detection limits. Note that the flare frequency varies by about a factor of 10 between the solar cycle maximum and minimum.

observed by Lin *et al.* (1984) during 141 min on June 27, 1980, agrees closely with the extrapolated frequency distribution of all flares observed by HXRBS in 1980. Note that the HXRBS peak flux distribution plotted by Lin *et al.* (1991), as derived from the

HXRBS peak rate distribution given by Dennis (1985), is too high by a factor of ~ 4. This difference resulted from the assumption of an E^{-5} average spectrum for all flares rather than using the best fit value for each flare as we have done here (see Section 3.6). At solar minimum, the extrapolation of the HXRBS frequency distribution for 1985 and 1986 falls below the 2σ upper limits of Lin's microflare search (Lin *et al.*, 1991) during the balloon flight on February 10–12, 1987. A systematic study of the variability of the flare rate as a function of the activity level during the solar cycle is in progress (Aschwanden and Dennis, 1993).

The observations of Datlowe *et al.* (1974) during October 1971 and June 1972, when solar activity level was about half of that from the previous solar maximum in 1968–1969, show a frequency distribution of 20 keV photon fluxes which are close to that obtained from HXRBS at solar minimum (1985–1986). Datlowe's dataset consists of 123 hard X-ray bursts recorded during 9 months, while HXRBS observed 545 flares in 1985–1986.

The drop-off of the flare frequency for bright flares with 20 keV photon fluxes above ~ 30 photons $\mathrm{cm}^{-2}\,\mathrm{s}^{-1}\,\mathrm{keV}^{-1}$ (corresponding to $\sim 3 \times 10^4$ counts s^{-1}) in the HXRBS frequency distributions may be related to the pulse pile-up characteristics of the instrument electronics. This effect results in a flatter spectrum and a correspondingly lower flux when extrapolated to 20 keV. A similar problem may exist for the instrument on OSO-7 used by Datlowe *et al.* (1974; see Figure 1 therein).

3.3. Peak energy flux (F) in nonthermal electrons

We calculate the energy in nonthermal electrons from the thick-target model. The power flux in nonthermal electrons deposited in a thick target is given by the following relation based on the formulae of Brown (1971):

$$F(>E_0) = 4.8 \times 10^{24} A E_0^{-\gamma+1} E_m^{\gamma} \gamma(\gamma-1)\beta(\gamma-\tfrac{1}{2},\tfrac{1}{2}) \text{ ergs s}^{-1}, \qquad (5)$$

where β is the beta function, and E_0 is the cut-off energy. The peak energy flux in electrons is computed for the time interval where the count rate has its maximum value.

Figure 5 shows the frequency distribution of the peak energy flux F (>25 keV) in electrons, with a power-law slope of -1.67 ± 0.04 between values of 10^{27} and 10^{29} ergs s^{-1}. The distribution shows a flattened plateau between 10^{24} and 10^{27} ergs s^{-1}. This results from the combined effect of missing events below 30 counts s^{-1} (see Section 3.1 and Figure 2) and the uncertainty of the spectral fit for weak events (<100 counts s^{-1} – see Figure 9). Thus, the range of values below the turnover is more extended than for the peak photon fux Φ (>25 keV) (Figure 3). The power-law slope for the peak energy distribution varies between -1.52 and -1.73 for different year groups (Table II).

3.4. Total energy (W) in nonthermal electrons

The total thick-target energy of a flare is calculated by summing over all the time intervals generated by the DCPFIT algorithm (see Section 2.2). Only flare intervals where the slope γ of the flare was greater than 1.1 or less than 7.0 are used in our calculations.

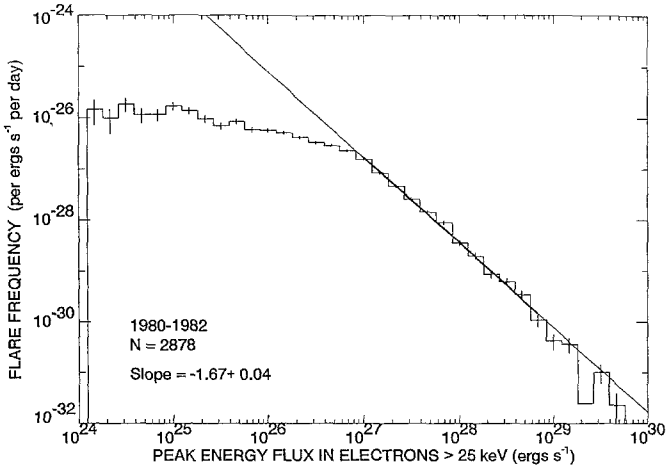

Fig. 5. Similar to Figure 3 except for the frequency distribution of the peak energy flux in electrons above 25 keV calculated assuming a thick-target model.

Values of $\gamma < 1.1$ correspond to a diverging energy integral, while values $\gamma > 7$ are beyond the capability of the instrument to measure and may reflect a steep thermal spectrum rather than the nonthermal thick-target situation.

We calculate the error δF_i of the thick-target flux F_i from the error propagation law and the uncertainties δA_i and $\delta \gamma_i$ determined from the power-law fit (Equation (3)):

$$\delta F_i = \sqrt{\left(\frac{\partial F_i}{\partial A_i}\right)^2 \delta A_i^2 + \left(\frac{\partial F_i}{\partial \gamma_i}\right)^2 \delta \gamma_i^2} \,. \tag{6}$$

An additional measure to avoid contributions from the thermal component later in flares and possible erroneous spectral fits both early and late in flares when the counting rate is low, we introduced the following second selection criteria for each time interval: only those intervals were included in the summation when the calculated value of the thick-target energy exceeded the mean value for all intervals, i.e.,

$$F_{\text{mean}} = \frac{\Sigma_i F_i \Delta t_i}{\Sigma_i \Delta t_i} \,, \tag{7}$$

where Δt_i is the duration of time interval i and the summation was over all intervals for which values of γ were obtained in the acceptable range ($1.1 < \gamma < 7$). The total thick-target energy $W(>E_0)$ in electrons for each flare is then given by

$$W(>E_0) = \Sigma_i F_i(>E_0)\Delta t_i \pm (\Sigma_i [\Delta F_i \Delta t_i]^2)^{1/2} \text{ ergs} \,, \tag{8}$$

where the summation includes only those time intervals for which $F_i > F_{\text{mean}}$ and γ lies in the acceptable range.

The resulting frequency distribution of W (> 25 keV) can be represented by a power-law function over the energy range of 5.10^{28} to 10^{32} ergs, i.e., over more than 3 decades

(Figure 6). The slope for the 1980–1982 data subset is -1.53 ± 0.02 with values consistent with this in all other data subsets (see Table II).

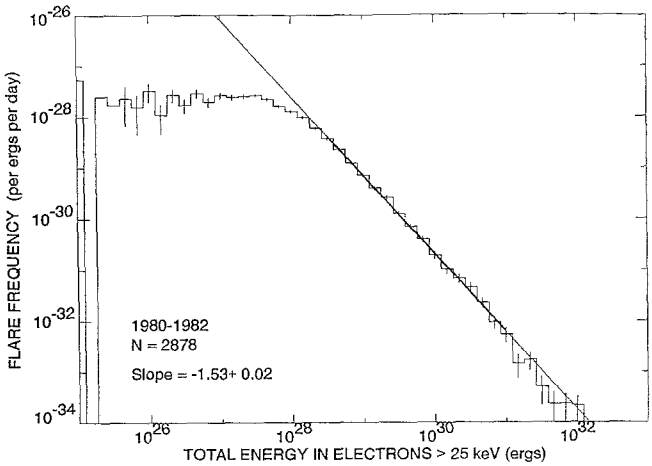

Fig. 6. The frequency distribution of the total energy in electrons above 25 keV calculated by integrating the thick-target energy rate over the flare duration.

3.5. TOTAL FLARE DURATION (D)

The frequency distributions of flare durations can be fitted with a power law for durations greater than 200 s. The power-law slope is -2.17 ± 0.05 for the range between 200 and 3000 s, for 1980–1982 (Figure 7), with a variation between -1.95 and -2.22 for different year groups (Table II). However, the distribution tends to steepen

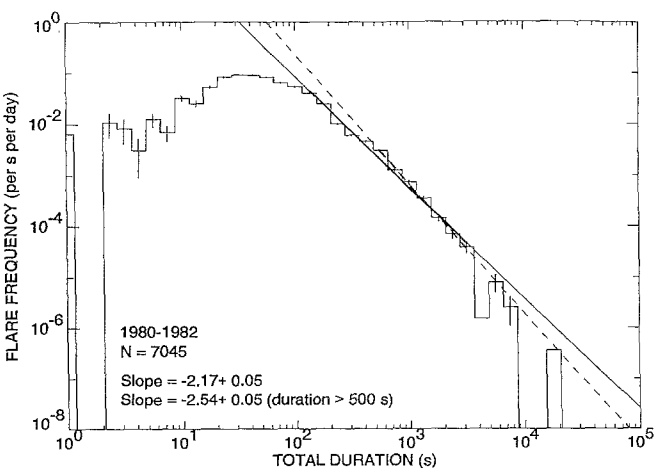

Fig. 7. The frequency distribution of the total flare duration for the same subset as in Figure 2. Note that the power law exhibits a trend to steepen with longer durations such that the slope changes from -2.17 to -2.54 in the interval from 200 to 3000 s (see Table II).

towards larger flare durations. A fit in the range of 500 to 2000 s indicates a steeper slope of -2.54 ± 0.05.

This steepening of the distribution may be a real effect but it could also be caused by two systematic effects resulting from the method of data selection. The first effect results from the fact that the duration of a flare was defined as the time interval when the HXR count rate was enhanced above the quiet background. This is usually longer than the time interval covered by the nonthermal component. The uncertainty in start and end time of the nonthermal component might explain why the frequency distribution of the flare duration shows larger deviations from an ideal power law than the thick-target energy flux F or total energy W. The second systematic effect is a consequence of the SMM orbit that gives a maximum length of uninterrupted observations, i.e., the 3.6×10^3 s daytime part of the orbit. Longer events can be identified if they are observed on the next orbit after the ~ 35 min nighttime period but this introduces a marked drop-off in the frequency distribution for longer durations.

The existence of a maximum in the frequency distribution at a duration of ~ 50 s results from the reduced sensitivity for detection of flares with peak background-subtracted rates below ~ 60 counts s^{-1} (see Section 3.1) and the general correlation between duration and peak rate (Section 3.6).

3.6. Correlations among flare parameters

We investigated the correlations between the five flare parameters P (peak rate), $I(25)$ (peak photon flux at 25 keV), Φ (>25) (peak photon flux above 25 keV), F (peak electron energy flux), W (total energy in nonthermal electrons), and D (total flare duration). Correlation scatter plots (on log-log scales) for some of the parameters are shown in Figures 8–11. We carried out a regression analysis to determine if any two parameters (X, Y) have a linear dependence in log-log space, i.e., if $\log Y(X) = \text{const.} + a \log X$ or $Y(X) \sim X^a$. Because of the considerable scatter and unknown systematic errors in the bivariate data sets, we have evaluated the functional relation between the variables by a least-squares fit method which treats the variables symmetrically, i.e., by minimizing the squares of the perpendicular distance to the linear regression fit ('orthogonal reduced major axis'; Isobe *et al.*, 1990). In addition, most of the correlations are affected by incomplete sampling for small events. The frequency distributions (Figures 2–7) show the parameter ranges where incomplete sampling affects the data, i.e., where deviations from a power-law distribution occur, resulting in a turn-over of the distribution. The cutoff values adopted for the correlation analysis are as follows: 100 counts s^{-1} for the peak count rate, 200 s for flare duration, 10^{27} ergs s^{-1} for the peak energy rate, and 10^{28} ergs for the total flare energy. In order to minimize the effects of this incomplete sampling in the linear regression fits, we defined a separatrix orthogonal to the regression line and intersecting it at the appropriate cutoff value of the parameter plotted along the x-axis. All events below and to the left of this separatrix were excluded from the regression analysis.

The parameters of the power-law regression functions between the parameters P, I, Φ, F, W, and D and their correlation coefficients are given in Table III. Noteworthy

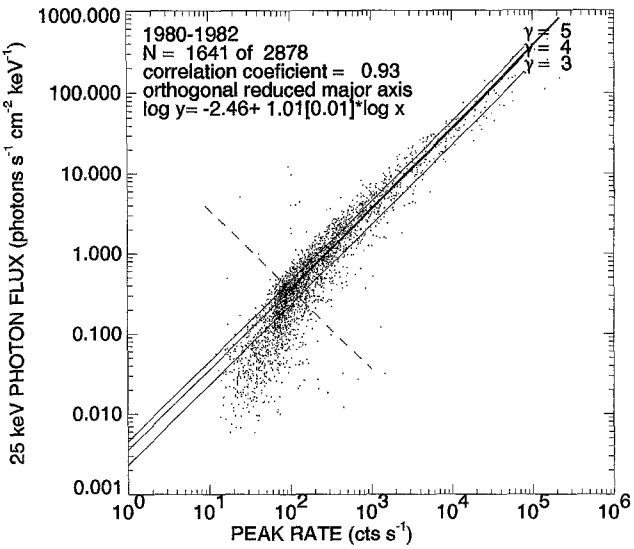

Fig. 8. Scatter plot of the 25-keV photon flux vs the peak count rate. The solid lines represent linear regression fits obtained by minimizing the orthogonal distance of the points from the fitted line. The dashed line represents the separatrix used to exclude data points for the least-squares fit in regions of incomplete sampling due to the instrument sensitivity limitations. The separatrix is defined by an orthogonal line to the fit with an intersection point at a peak rate of 100 counts s^{-1}. The linear fit in log-log space represents a power-law relation of $y(x) \sim x^{1.01 \pm 0.01}$ and a correlation coefficient of 0.93. The overlayed thin lines labeled as $\gamma = 3$, 4, and 5, represent calculated photon fluxes for photon spectra with slopes of 3–5 based on the HXRBS instrumental response function. Note that the regression fit is coaligned with the line corresponding to a spectral slope of 4.

correlations (with a correlation coefficient of > 0.75) exist between P and I, Φ, F, and W, but no strong correlation was found between the flare duration D and any other parameter.

The 25 keV peak photon flux shows a correlation with the peak count rate P of $I(25) \sim 3.5 \times 10^{-2} P^{1.01}$ (Figure 8), with a correlation coefficient of 0.93. Thus, the conversion of the peak count rate to the 25 keV photon flux is nearly linear, and the slight dependence of the spectral index on the peak count rate does not introduce a significant deviation from the linear relationship. The dependence on the power-law index γ of the HXR photon spectrum is indicated in Figure 8 for slopes of $\gamma = 3$, 4, and 5. The linear regression fit is most consistent with an average spectral index $\gamma = 4$. In this context, we can correct an earlier published value for the 20 keV photon flux conversion, i.e., 30 photons $cm^{-2}\ s^{-1}\ keV^{-1}$ for a count rate of 1000 counts s^{-1} and a mean spectral slope of 5, given in Dennis (1985). Based on the statistics of spectral parameters from the flares in 1980–1982, we find a value of $I(20) \sim 15$ photons $cm^{-2}\ s^{-1}\ keV^{-1}$ for the same spectral index of 5, or a value of $I(20) \sim 8$ photons $cm^{-2}\ s^{-1}\ keV^{-1}$ for the more typical spectral slope of 4.

The peak energy flux F in electrons as a function of peak rate P, presented in Figure 9, follows the relation $F \sim P^{0.94 \pm 0.02}$, which again corresponds to a nearly linear relation. The linear regression fit in the scatter plot (Figure 9) is affected by incomplete sampling

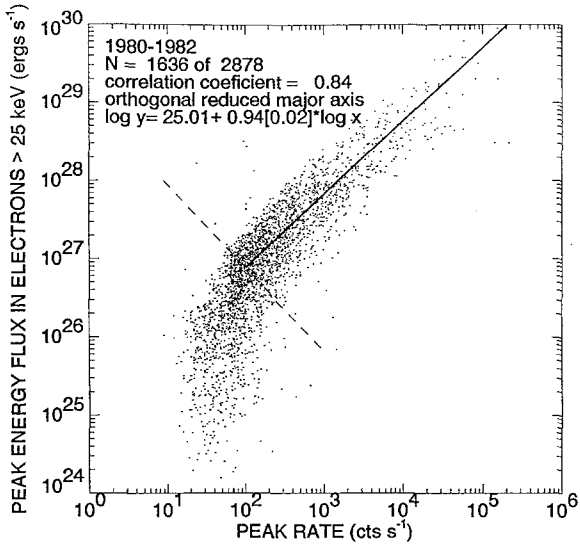

Fig. 9. Scatter plot similar to Figure 8 for the peak energy flux in electrons > 25 keV vs peak count rate.

for spectral slopes of $\gamma > 7$ and for peak rates $P < 100$ counts s^{-1}. Thus, the peak energy flux F in electrons can be considered, in first order, to be proportional to the count rate P or to the photon flux I or Φ, in the statistical average.

The total (thick-target) energy, W, exhibits a correlation of $W \sim P^{1.25 \pm 0.02}$ with a correlation coefficient of 0.79 (Figure 10). The flare duration, D, which is only weakly correlated with P (correlation coefficient = 0.32, see Table III), introduces considerable

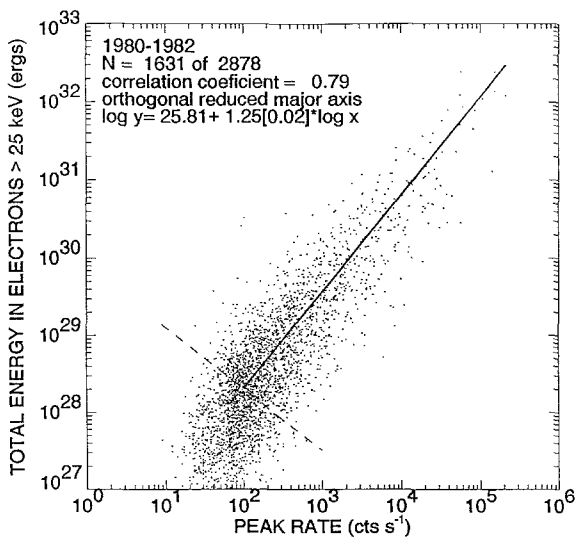

Fig. 10. Scatter plot similar to Figure 8 for the total flare energy W versus peak rate.

scatter in the correlation of the time-integrated parameter W with P (Figure 10). The exponent a of the correlation $W \sim P^a$ varies between 1.21 and 1.31 if determined using different methods or in different energy ranges. Thus, the total flare energy does not scale proportionally with the peak count rate.

In addition, we find a strong correlation (with a correlation coefficient of 0.92) between the total energy W and the product of the peak energy flux F times the flare duration D (Figure 11), i.e., $F \times D \sim W^{1.18 \pm 0.01}$, obtained above a cutoff of

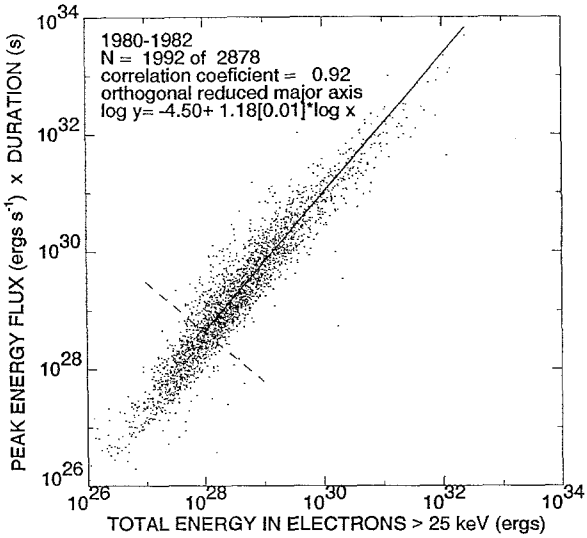

Fig. 11. Scatter plot of the total energy W in electrons with energies above 25 keV versus the product of the peak energy flux F in electrons above 25 keV and the total flare duration D.

$W > 10^{28}$ ergs. The exact value of the exponent in the correlation depends on this cutoff energy, either because of undersampling at weak flares or because of a real systematic trend in the functional relationship. For the biggest events, pulse pile-up could contribute to this deviation from a power-law relation.

3.7. Effect of the Solar Cycle and Instrumental Gain Variations

Examination of Table II suggests that there is some variability of the power-law slope of the frequency distribution of most of the parameters during the solar cycle from 1980 through 1989. These changes may be caused by the variable level of solar activity or by instrumental effects. In Figure 12 we show the variability of the slope of the frequency distribution of the photon flux at 25 keV, $I(25)$, and at 50 keV, $I(50)$, for each year. The slope was determined by fitting an identical range each year, i.e., in the range of 0.2–20 photons $cm^{-2}\ s^{-1}\ keV^{-1}$ for $I(25)$ and 0.01–2.0 photons $cm^{-2}\ s^{-1}\ keV^{-1}$ for 50 keV. On time scales of 2–3 years, the variability of the slope is less than the statistical uncertainty of the linear regression fit (Figure 12). However, there is a significant variability in the slopes for individual years. It is not clear whether this variability is due

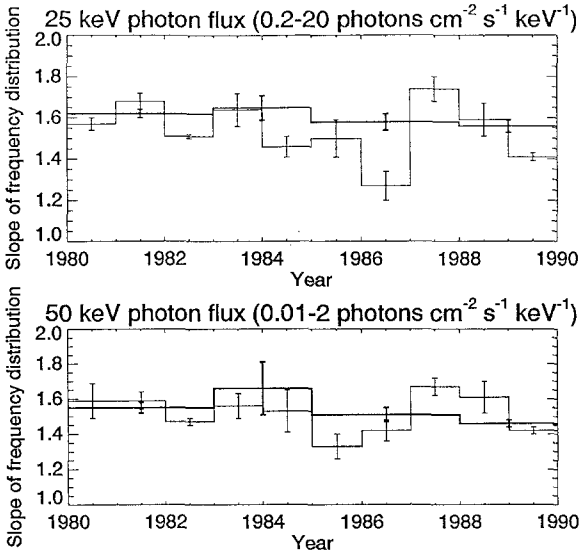

Fig. 12. Variability of the power-law slope of the frequency distribution of the 25 keV (*top*) and 50 keV (*bottom*) photon flux during the years 1980 through 1989. The error bars represent the statistical uncertainty of the linear regression fit. The years are combined according to the intervals given in Table II (thick lines).

to systematic trends associated with the phase of the solar cycle, to time periods of high activity on time scales less than a year, or to instrumental effects. Although there is a trend for flatter slopes in the years 1984–1986 around the solar cycle minimum, there is also a systematic flattening of the slope during the rise phase of the solar cycle maximum from 1987 to 1989. We suspect that this systematic trend is at least partially an effect of the change of the gain state of HXRBS after 1986. The threshold energy increased from ~ 25 to ~ 50 keV in the late years of the SMM mission, and this caused a decrease in the detection efficiency for weak flares with energies < 50 keV. Since the ratio of weak flares to strong flares determines the slope of the frequency distribution, the rise of the instrumental threshold is expected to result in a flatter slope. We observe, indeed, a systematic flattening of the slope by $\sim 25\%$ from 1987 to 1989. However, the variability of the slope due to the solar cycle shows even larger changes, e.g., a jump by $\sim 40\%$ from 1986 to 1987.

No consistent relationship is found between the slope of the frequency distribution of the HXR photon flux (Figure 12) and the flare frequency (Figure 1). On one hand, the flattest slopes are found during solar minimum, i.e., in 1986 for the 25 keV photon fux and in 1985 for the 50 keV flux. On the other hand, the highest flare frequency is found in 1982 and in 1989, where the slope of the frequency distribution is significantly flatter than in the preceding or following year. Since the variability of the slope is larger on a time scale of 1 year than it is on a scale of 3 years, we expect that the slope of the frequency distribution varies on even shorter time scales. Bai (1992) found a dependence of the variability of the frequency distribution of the peak count rate on the phase of

the 154-day period. For a more detailed investigation of the variability of frequency distributions of HXR parameters as function of the solar cycle and the level of solar activity, we refer to a separate study currently in progress (Aschwanden and Dennis, 1992b).

4. Discussion

All investigated flare parameters show power-law frequency distributions over two to three decades, and some flare parameters are strongly correlated with others. First, we discuss the relations between frequency distributions implied by the parameter correlations (Section 4.1). Then, in Section 4.2, we discuss the power-law slope of the frequency distributions in terms of the exponential energy build-up model of Rosner and Vaiana (1978). Another approach to understand the nature of frequency distributions in flare parameters in terms of avalanche models and nonlinear systems with self-organized criticality, is discussed in Section 4.3.

4.1. Frequency distributions and correlated parameters

The frequency distributions of two flare parameter X and Y do not reveal, by themselves, whether the parameters are correlated or not. However, if a correlation does exist, a one-parameter functional dependence can be derived from the slopes of the two frequency distributions. In particular, if the correlation function follows a simple power law, i.e., $Y(X) \sim X^{-c}$, the exponent c obeys the relation

$$c = (a - 1)/(b - 1)\,, \tag{9}$$

where a and b are the power-law slopes of the X and Y frequency distributions respectively, i.e., $N(X) \sim X^{-a}$ and $N(Y) \sim Y^{-b}$. This can be shown by substituting the function $Y(X)$ into the distribution $N(X)\,\mathrm{d}X = N[Y(X)]\,(\mathrm{d}Y/\mathrm{d}X)\,\mathrm{d}X$. The values of the exponents c calculated from Equation (9) using the values of the power-law slopes a and b listed in Table II are compiled in Table III for comparison with the values found from the regression analysis. The calculated values can be used as consistency checks for the functional dependences found by least-squares fit methods. Because the relations defined by Equation (9) are derived from the power-law slopes for parameter ranges above the sensitivity threshold, they are not affected by incomplete sampling below this threshold. Table III shows the close agreement between the power-law slopes obtained from both methods. The agreement is generally better the higher the correlation coefficient. Because the slope of the frequency distributions and the linear regression fits sometime show a systematic trend to deviate from power laws for some parameters, we performed these calculations for all flares above two different thresholds (listed in Table II). The two cases are denoted as 'all flares' and 'strong flares' in Table III.

The strong correlation found between the total energy W and the product $F \times D$ of the peak energy rate times the flare duration provides a useful relation to estimate the total flare energy without carrying out the tedious time integration of energy spectra over the entire flare duration. A similar relation has been derived from a general energy dissipation model based on the dynamics of a nonlinear relaxation process characterized

by a 'logistic equation' (Aschwanden, 1992). This model predicts a relation $W = F \times T$, where T is the duration of the energy dissipation process when the energy dissipation rate was $>42\%$ of its peak value. The empirical correlation $W^{1.18} \sim F \times D$ suggests that the flare duration D is not exactly proportional to the duration T of the energy dissipation process. From the theoretical prediction that $W = F \times T$ and the empirically found correlation $F_{30} \times D = 8W_{30}^{1.18}$, with F_{30} and W_{30} in units of 10^{30} ergs s^{-1} and 10^{30} ergs, respectively, we derive the relation

$$T = D(0.125W_{30}^{-0.18}) . \tag{10}$$

For instance, we find $T = 0.3D$ for weak flares ($W = 10^{28}$ ergs), $T = 0.1D$ for moderate flares ($W = 10^{30}$ ergs), and $T = 0.05D$ for large flares ($W = 10^{32}$ ergs). Thus, the measured flare duration, D, which is defined as the time interval of enhanced HXR emission above the background level, encompasses a time scale which is systematically longer than the duration of the energy dissipation process predicted by the logistic model, a factor of 3 longer for weak flares, and up to 20 times longer for large flares. This prediction can be tested by measuring the FWHM of non-thermal flare structures, say above 50 keV, and comparing them with the standard flare duration, D.

The correlation $F \times D \sim W^{1.18}$ obtained from the correlation analysis implies that the three frequency distributions $N(W)$, $N(F)$, and $N(D)$ are not independent, e.g., the slope of $N(W)$ can be calculated from the slopes of $N(F)$ and $N(D)$ using Equation (9). Using the slopes of these frequency distributions given in Table II, we find the relation $F \times D \sim W^{1.21}$ (Table III), which is in close agreement with the result obtained from the correlation analysis.

4.2. Statistical models for flare energy build-up and release

Rosner and Vaiana (1978) studied frequency distributions of flares from the Sun, flare stars, and transient sources. They found the following two results: (i) in every case, there exists an energy range in which the flaring frequency is well described by a power-law behavior as a function of the energy released, and (ii) deviations from power-law behavior occur only at the low energy end of the frequency distribution. They developed a model in which information about the rate of energy storage and energy release was included. The model was based on the following three assumptions: (i) the energy build-up is exponential between flares, (ii) flaring is a stochastic process, and (iii) all the free energy built up between flares is released by the following flare. The flare energy release is considered as a relaxation process of the locally accumulated free magnetic energy. The probability $p(t)$ for a flare to begin in the time interval between t and $t + \mathrm{d}t$ can be determined from Poisson statistics, i.e., $\mathrm{d}p(t) = (1/t_f) \exp(-t/t_f)\, \mathrm{d}t$, where t_f is the mean time between flares. The system returns to its unperturbed state after the flare. Distinct flaring regions in the source are assumed to be physically uncoupled, i.e., the flares are independent of each other. These two assumptions, the exponential growth of free energy $W(t)$ and the stochastic distribution of flaring times $N(t) \sim p(t)$, lead to a power law for the frequency distribution of flare energies, $N(W) \sim W^{-s}$. Provided that a proportional amount of the accumulated magnetic energy is converted into accelera-

tion of energetic particles, we expect also a power law for the frequency distribution of the total energy of injected electrons, such as derived from the hard X-ray fluence in terms of the thick-target model. Besides the pioneering observations of Datlowe *et al.* (1974) and Lin *et al.* (1984), we confirm the power-law shape of the frequency distribution for flare energies with large statistics (> 8000 flares), over a range of almost four decades in energy (10^{28}–10^{32} ergs). Thus, the observed flare energies derived from HXR's are fully consistent with the exponential energy build-up model of Rosner and Vaiana (1978).

Following the model of Rosner and Vaiana (1978), the slope s of the frequency distribution of flaring energies represents a function of the ratio of the average time between flares t_f to the e-folding energy build-up time t_b, i.e., $s = (t_b/t_f + 1)$. From our best value of $s = 1.53$ for flare energies W (> 25 keV) (see Table II), we find a ratio of $t_f/t_b = 1.9$. The average dissipated energy per flare can then be expressed in terms of the quiescent level W_Q by the exponential relation $W/W_Q = \exp[1/(s-1)] - 1$, i.e., a one-parameter function of the power-law slope s (Aschwanden, 1992). For solar cycle 21, we found no significant variation, with $s = 1.53 \pm 0.02$ at the maximum in 1980, and 1.48 ± 0.02 at the minimum in 1985–1987 (Table II). This corresponds to an average dissipated energy of

$$W/W_Q = \exp(1/0.53) - 1 = 5.6 \quad \text{at solar maximum, and to}$$

$$W/W_Q = \exp(1/0.48) - 1 = 7.0 \quad \text{at solar minimum .}$$

Although the flaring rate varied by a factor of ~ 20 (Figure 1) between solar maximum and minimum, the average dissipated energy (W/W_Q) per flare stays constant within uncertainties. How can we explain this constancy in s and, hence, also in W/W_Q, given that $s = (t_b/t_f - 1)$? Since the sunspot number varies by a factor of ~ 10–20 during the solar cycle, the variation of the overall flaring rate by a factor of ~ 20 (Figure 1) is likely to be due to the variable number of active regions, while the average flaring rate per active region ($1/t_f$) may be constant. If this is the case then, to preserve the constancy of s, the magnetic energy build-up time t_b must also be constant and not sensitive to the level of solar activity.

Solar flares exhibit very similar frequency distributions at different wavelengths (see Table I), such as in radio, soft X-rays or hard X-rays. The slope of the power-law frequency distribution is typically 1.7–1.8 for the peak count rate (or peak flux), 1.4–1.6 for flare energies, and ~ 2.0 for flare durations. Aschwanden and Dennis (1992) showed that elementary flare time structures exhibit different frequency distributions for various time scales between 0.1 and 20 s. The result of this study was that the average dissipated energy (according to Rosner and Vaiana's model) follows a reciprocal dependence on the time scale of the elementary structures, with the shortest structures exhibiting the flattest frequency distributions and being associated with the greatest fractional energy releases (W/W_Q).

Hudson (1978) pointed out that the frequency distribution of interplanetary proton events (Van Hollebeke, Sung, and McDonald, 1975) has a much flatter slope than that

of a representative dataset of typical solar flares. He concluded that the functional dependence between the two slopes (Equation (9)) implies an energy threshold for proton production. Aschwanden (1992) discusses the peak-rate frequency distributions found for different flare-associated phenomena and calculates the resulting frequency distributions for flare energies. For the case of interplanetary proton events, we find a ratio of $W/W_Q > 200$ suggesting that these events are preferentially associated with very energetic flares. Cliver *et al.* (1991) finds a slope of 1.30 for interplanetary 3.6–18 MeV electrons corresponding to $W/W_Q = 20$ (see Table I in Aschwanden, 1992).

4.3. Avalanche models and self-organized criticality

Another approach to understanding the frequency distributions of flare parameters proposed by Lu and Hamilton (1991) is based on the assumption that the solar coronal magnetic field is in a self-organized critical state and that a solar flare is the nonlinear response of many small reconnection events. Self-organized criticality is a concept that characterizes the behavior of dissipative systems that contain a large number of elements that interact over a short range. 'Many composite systems naturally evolve to a critical state in which a minor event starts a chain reaction that can affect any number of elements in the system' (Bak and Chen, 1991). A more detailed description of avalanche theory can be found in Bak, Tang, and Wiesenfeld (1988), Bak, Chen, and Creutz (1989), and Bak and Chen (1991).

Lu and Hamilton (1991) applied this avalanche theory to solar flares on the assumption that the energy released during a flare is the result of explosive magnetic reconnection. Parker (1988) suggested that reconnection in a magnetized plasma will normally proceed slowly when the magnetic discontinuity angle τ between adjacent magnetic field vectors is less than some critical angle. If the angle becomes greater than this critical angle at some location, reconnection will take place more rapidly at that point. If the resulting release of energy and its transport to neighboring locations results in increasing the magnetic angle to $> \tau$ at other sites, then a chain reaction or avalanche can occur. This can produce an explosive release of a large fraction of the free energy stored in the magnetic field, i.e., a solar flare.

In Lu and Hamilton's (1991) approach, each flare is considered as an avalanche event in a critically stable system. They simulated the relaxation of randomly disturbed magnetic fields that could locally exceed the threshold of a critical shear angle τ and found power-law distributions for the dissipated energies and time scales of such avalanche events. Based on these simulations, they predicted the following slopes for the power-law parts of the frequency distributions: ~ 1.8 for the peak dissipation rate, ~ 1.4 for the dissipated energy, and ~ 2.0 for the duration of the energy dissipation process. These values are in close agreement with the values obtained from our HXRBS flare data set in terms of the thick-target model. Bai (1992) criticized the Lu and Hamilton model, pointing out that the shape of the frequency distributions of flare parameters is not constant during the solar cycle, and thus violates the universality of the concept of self-organized criticality. However, we do not consider the slope of the frequency distribution of a given flare parameter to be a universal constant. For example,

in Section 4.2, we discussed a physical model which relates the slope of the frequency distribution to the ratio of time scales for energy buildup and flaring, and this ratio may change during the solar activity cycle, producing a corresponding change in the frequency distribution.

5. Summary and Conclusions

5.1. Observational summary

We have determined the frequency distributions and correlations of hard X-ray parameters from over 12000 solar flares recorded with HXRBS on SMM from 1980 to 1989. The directly measured flare parameters used in the analysis include the peak count rate and flare duration from all 12000 flares. Derived parameters were obtained for about 8000 flares where reliable power-law fits could be obtained to the energy spectra throughout the flare. These derived parameters include the peak photon fluxes at and above 25 keV, and the peak energy and total flare energy in electrons above 25 keV calculated assuming a thick-target model. We find that all HXR parameters measured at the time of the peak counting rate for each flare (i.e., count rate, photon flux, and electron flux) show a frequency distribution which can be represented by a power-law over about 3 orders of magnitude with a similar slope between -1.6 and -1.7. The frequency distribution of the total flare energy also can be represented by a power-law over 3 orders of magnitude but with a flatter slope of ~ -1.5. For the total flare duration, which is expected to be completely sampled in the range of 200–2000 s, we find a frequency distribution that shows a trend of a steepening power-law slope toward longer flare durations, i.e., from -2.0 at 200 s to -2.6 at 2000 s.

Due to the possible variability of these parameter distributions with time during the solar cycle and with instrumental gain changes, we subdivided the total data set into different groups of years. The data set from 1980 through 1982 contains the best statistics and constancy of instrumental operation. The following slopes were determined for this restricted data set from power-law fits to the frequency distributions of the different flare parameters:

peak count rate	P	-1.73 ± 0.01,
total duration	D	-2.17 ± 0.05,
peak hard X-ray flux at 25 keV	$I(25\text{ keV})$	-1.62 ± 0.02,
peak hard X-ray flux >25 keV	$\Phi\ (>25\text{ keV})$	-1.59 ± 0.01,
peak energy flux in electrons	$F\ (>25\text{ keV})$	-1.67 ± 0.04,
total energy in electrons	$W\ (>25\text{ keV})$	-1.53 ± 0.02.

Although the flaring rate varies by about a factor of 20 during the solar cycle, there is no significant long-term variation in the slope of the frequency distributions for different solar cycles or phases of the solar cycle. This indicates that the mechanism responsible

for determining the relative size of flares is insensitive to the level of solar activity. There are indications of variability in the slope of the frequency distributions on time scales ≤ 1 year that may be related to the solar activity. However, a clear trend could not be established because of poor statistics in years with low solar activity.

All of the analyzed flare parameters are strongly correlated with the peak count rate (with a correlation coefficient between 0.77 and 0.95), except for the flare duration (with a correlation coefficient of 0.32). The following correlations were established by means of linear regression analysis and frequency distributions (ignoring incompletely sampled weak flares with count rates ≤ 100 counts s^{-1}):

$$I(25\ \text{keV}) \sim P^{1.01},$$

$$\Phi\ (>25\ \text{keV}) \sim P^{1.07},$$

$$F\ (>25\ \text{keV}) \sim P^{0.94},$$

$$W\ (>25\ \text{keV}) \sim P^{1.25},$$

$$F \times D\ (>25\ \text{keV}) \sim W^{1.18}.$$

These correlations imply a functional dependence between the power-law slope of the frequency distributions of the flare parameters Φ, P, F, and W, which have been consistently reproduced with two different methods (see Table III). Using the predictions of a 'logistic' model for energy dissipation proposed by Aschwanden (1992), we find that the duration of the energy release process is a factor of ~ 3 shorter than the measured flare duration D in hard X-rays for weak flares and a factor of ~ 20 times shorter for large flares. This presumably results from the greater contribution to the hard X-ray flux from the heated plasma in the larger flares.

5.2. Conclusions

All of the HXR flare parameters (except for the flare duration) show a power-law frequency distribution extending over 3 decades above the threshold implied by instrumental sensitivity. The confirmation of a power-law shape for the frequency distribution of flare energies is fully consistent with the model of Rosner and Vaiana (1978), implying that the flare energy build-up essentially is governed by exponential growth, under the assumption of stochastic flaring. The absolute value of the power-law slope can be related to an average amount of dissipated flare energy in terms of the quiescent level in their model. For solar flares, we find an average dissipated energy of 5–7 times the quiescent level, and a ratio of 1.9 between the average time t_f between subsequent flares (at the same flare site) and the e-folding energy build-up time t_b. This ratio has been found to be stable during the solar activity cycle if biannual averages are used but there are indications of variability on shorter time scales. The power-law form and the slope of the flare parameter frequency distributions are also consistent with the concept of self-organized criticality in avalanche models, where power-law distributions have been found from simulations using a simple magnetic relaxation model (Lu and Hamilton, 1991).

Acknowledgements

N.C. thanks Richard Schwartz and Dominic Zarro for inspiring discussions and guidance, Russ Hamilton and Ed Lu for helpful discussions, and the people in the Solar Data Analysis Center at Goddard Space Flight Center for their generous support. This work was done under NASA grant NAS5-30442 through USRA and with support from the 1991/1992 SMM/GI program.

References

Akabane, K.: 956, *Publ. Astron. Soc. Japan* **8**, Nos. 3–4.
Aschwanden, M. J.: 1992, *Astrophys. J.* (submitted).
Aschwanden, M. J. and Dennis, B. R.: 1992, *Astrophys. J.* (submitted).
Aschwanden, M. J. an Dennis, B. R.: 1993, *Solar Phys.* (in preparation).
Aschwanden, M. J. and Klimchuk, J. A.: 1992, *Astrophys. J.* (in preparation).
Bai, T.: 1992 (submitted).
Bak, P. and Chen, K.: 1991, *Sci. Amer.* **46**.
Bak, P., Chen, K., and Creutz, M.: 1989, *Nature* **342**, 780.
Bak, P., Tang, C., and Wiesenfeld, K.: 1988, *Phys. Rev.* **A38/1**, 364.
Batchelor, D. A.: 1984, Ph.D. Dissertation, U. N. Carolina Chapel Hill, NASA Technical Memorandum 86102.
Brown, J. C.: 1971, *Solar Phys.* **18**, 489.
Cliver, E., Reames, D., Kahler, S., and Cane, H.: 1991, *Proc. 22nd Int. Cosmic Roy. Conf., Dublin* **3**, 25.
Datlowe, D. W., Elcan, M. J., and Hudson, H. S.: 1974, *Solar Phys.* **39**, 155.
Dennis, B. R.: 1985, *Solar Phys.* **100**, 465.
Dennis, B. R., Orwig, L. E., Kennard, G. S., Labow, G. J., Schwartz, R. A., Shaver, A. R., and Tolbert, A. K.: 1991, *NASA Technical Memorandum* **4332**.
Drake, J. F.: 1971, *Solar Phys.* **16**, 152.
Fitzenreiter, R. J., Fainberg, J., and Bundy, R. B., 1976, *Solar Phys.* **46**, 465.
Isobe, T., Feigelson, E. D., Akritas, M. G., and Babu, G. J.: 1990, *Astrophys. J.* **364**, 104.
Hudson, H. S.: 1978, *Solar Phys.* **57**, 237.
Hudson, H. S., Peterson, L. E., and Schwartz, D. A.: 1969, *Astrophys. J.* **157**, 389.
Lin, R. P., Hurley, K. C., Smith, D. M., and Pelling, R. M.: 1991, *Solar Phys.* **135**, 57.
Lin, R. P., Schwartz, R. A., Kane, S. R., Pelling, R. M., and Hurley, K. C.: 1984, *Astrophys. J.* **283**, 421.
Lu, E. T. and Hamilton, R. J.: 1991, *Astrophys. J.* **380**, L89.
Orwig, L. E., Frost, K. J., and Dennis, B. R.: 1980, *Solar Phys.* **65**, 25.
Parker, E. N.: 1988, *Astrophys. J.* **330**, 474.
Rosner, R. and Vaiana, G. S.: 1978, *Astrophys. J.* **222**, 1104.
Schwartz, R. A., Orwig, L. E., Dennis, B. R., Ling, J. C., and Wheaton, W. A.: 1991, *Astrophys. J.* **376**, 312.
Speich, D. M., Nelson, J. J., Licata, J. P., and Tolbert, A. K.: 1991, *NASA Technical Memorandum* **4287**.
Van Hollebeke, M. A. I., Sung, L. S., and McDonald, F. B.: 1975, *Solar Phys.* **41**, 189.